observed after high-energy irradiation of these materials[18,19]. The present diffusion study provides additional evidence for this physical concept, and illustrates the strong correlation between atomic mass transport processes and electronic properties of native defects in semiconductors. □

Received 6 July; accepted 11 September 2000.

1. *Landolt-Börnstein, New Series, Group III*, Vol. 26, Pt B, *Diffusion in Solid Metals and Alloys* (ed. Mehrer, H.) (Springer, Berlin, 1990).
2. *Landolt-Börnstein, New Series, Group III*, Vol. 33, Pt A *Diffusion in Semiconductors* (ed. Beke, D. L.) (Springer, Berlin, 1998).
3. Fuchs, H. D. *et al.* ^{70}Ge/ ^{74}Ge isotope heterostructures: an approach to self-diffusion studies. *Phys. Rev. B* **51,** 16817–16821 (1995).
4. Bracht, H., Haller, E. E. & Clark-Phelps, R. Silicon self-diffusion in isotope heterostructures. *Phys. Rev. Lett.* **81,** 393–396 (1998).
5. Wang, L. *et al.* Ga self-diffusion in GaAs isotope heterostructures. *Phys. Rev. Lett.* **76,** 2342–2345 (1996).
6. Bracht, H., Norseng, M., Haller, E. E., Eberl, K. & Cardona, M. Enhanced and retarded Ga self-diffusion in Si and Be doped GaAs isotope heterostructures. *Solid State Commun.* **112,** 301–314 (1999).
7. Wang, L. *et al.* Gallium self-diffusion in gallium phosphide. *Appl. Phys. Lett.* **70,** 1831–1833 (1997).
8. Mathiot, D. & Edelin, G. Diffusion of indium in GaSb. *Phil. Mag. A* **41,** 447–458 (1980).
9. Edelin, G. & Mathiot, D. A model for the determination of the defect concentrations in III-V compounds: The case of GaSb. *Phil. Mag. A* **42,** 95–110 (1980).
10. Gude, A. & Mehrer, H. Diffusion in the $D0_3$-type intermetallic phase Fe_3Si. *Phil. Mag. A* **76,** 1–29 (1997).
11. Salamon, M. & Mehrer, H. Diffusion in the B20-type phase FeSi. *Phil. Mag. A* **79,** 2137–2155 (1999).
12. Bösker, G. *et al.* Arsenic diffusion in intrinsic gallium arsenide. *Mater. Res. Soc. Symp. Proc.* **527,** 347–356 (1998).
13. Weiler, D. & Mehrer, H. Self-diffusion of gallium and antimony in GaSb. *Phil. Mag. A* **49,** 309–325 (1984).
14. Tang, X.-P., Geyer, U., Busch, R., Johnson, W. L. & Wu, Y. Diffusion mechanisms in metallic supercooled liquids and glasses. *Nature* **402,** 160–162 (1999).
15. Talwar, D. N. & Ting, C. S. Tight-binding calculations for the electronic structure of isolated vacancies and impurities in III-V compound semiconductors. *Phys. Rev. B* **25,** 2660–2680 (1982).
16. Xu, H. Electronic structure of neutral and charged vacancies in Ga-related III-V compound semiconductors. *J. Appl. Phys.* **68,** 4077–4086 (1990).
17. Kühn, W., Strehlow, R. & Hanke, M. Self-consistent tight-binding investigation of chemical trends for native defects in III-V semiconductors. *Phys. Status Solidi B* **151,** 541–557 (1987).
18. Walukiewicz, W. Mechanism of Fermi level stabilization in semiconductors. *Phys. Rev. B* **37,** 4760–4763 (1988).
19. Walukiewicz, W. Amphoteric native defects in semiconductors. *Appl. Phys. Lett.* **54,** 2094–2096 (1989).

Acknowledgements

H.B. acknowledges a Feodor Lynen fellowship from the Alexander von Humboldt-Stiftung. This work was supported in part by the Office of Energy Research, Office of Basic Energy Sciences, Materials Science Division of the US Department of Energy, and the US National Science Foundation.

Correspondence and requests for materials should be addressed to H.B. (e-mail: bracht@uni-muenster.de) or to E.E.H. (e-mail: eehaller@lbl.gov).

Early onset and tropical forcing of 100,000-year Pleistocene glacial cycles

Scott Rutherford & Steven D'Hondt

University of Rhode Island, Graduate School of Oceanography, Narragansett, Rhode Island 02882, USA

Between 1.5 and 0.6 Myr ago, the period of the Earth's glacial cycles changed from 41 kyr, the period of the Earth's obliquity cycles, to 100 kyr, the period of the Earth's orbital eccentricity[1,2], which has a much smaller effect on global insolation. The timing of this transition and its causes pose one of the most perplexing problems in palaeoclimate research[3]. Here we use complex demodulation to examine the phase evolution of precession and semiprecession cycles—the latter of which are phase-coupled to both precession and eccentricity—in the tropical and extratropical Atlantic Ocean. We find that about 1.5 Myr ago, tropical semiprecession cycles (with periods of about 11.5 kyr) started to propagate to higher latitudes, coincident with a growing amplitude envelope of the 100-kyr cycles. Evidence from numerical models suggests that cycles of about 10 kyr in length may be required to explain the high amplitude of the 100-kyr cycles[4]. Combining our results with consideration of a modern analogue, we conclude that increased heat flow across the equator or from the tropics to higher latitudes around 1.5 Myr ago strengthened the semiprecession cycle in the Northern Hemisphere, and triggered the transition to sustained 100-kyr glacial cycles.

The 100-kyr band of global ice-volume variability exhibits several significant features over the past 2.6 Myr (Fig. 1a). What are generally regarded as the late Pleistocene glacial cycles began about 0.6 Myr ago and the first high-amplitude 100-kyr variability began about 1.2 Myr ago[5]. Inspection of the filtered record shows that the amplitude envelope of the 100-kyr cycle began to expand toward late Pleistocene values 1.4–1.5 Myr ago. Before then, 100-kyr cycles occurred but were not sustained.

This interpretation is supported by an elegant study of the amplitude and phase of the $\delta^{18}O$ record at two major eccentricity periods (95 and 124 kyr)[6]. The study showed that frequency modulation of $\delta^{18}O$ in the eccentricity band, which is characteristic of the late Pleistocene[7], and the phase lock between $\delta^{18}O$ and orbital eccentricity began near 1.5 Myr ago[6]. Furthermore, although its temporal resolution is limited, another study showed that the asymmetry (a third-moment quantity that describes the shape of a time series) of the $\delta^{18}O$ record changed dramatically 1.5 Myr ago[8].

The timing of this transition coincided with other events

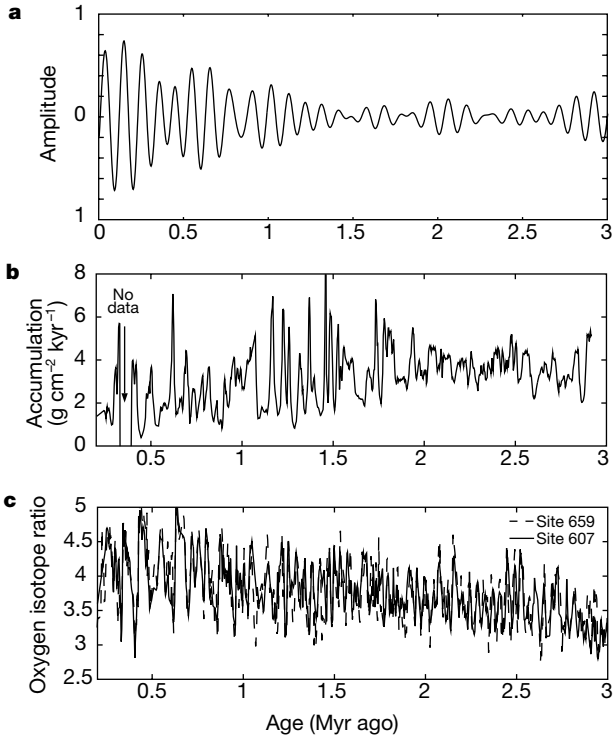

Figure 1 Oxygen isotope and calcium carbonate accumulation time series. **a**, Bandpass filter of the Site 659 $\delta^{18}O$ record. Periods between 90 and 130 kyr are passed by the filter. We note that the band begins to oscillate consistently and increase in amplitude near 1.5 Myr ago. **b**, Calcium carbonate mass accumulation for Site 607. Mass accumulation is calculated from weight per cent carbonate[27,2], wet bulk density measured by the Gamma Ray Attenuation Porosity Evaluator, grain density[30] and sedimentation rate calculated from the oxygen isotope age model. We note the change in the character of $CaCO_3$ accumulation that occurs near 1.5 Myr ago. **c**, $\delta^{18}O$ record from Site 607 correlated to $\delta^{18}O$ from Site 659.

observed in the palaeoclimate record. At about 1.6 Myr ago, glacial–interglacial $\delta^{13}C$ variations and dissolution of $CaCO_3$ in the tropical Atlantic indicate the first substantial decrease in North Atlantic Deep Water (NADW) production during glacial periods[9,10]. Palaeoclimate records of the Asian monsoon exhibit major phase changes relative to insolation[11] and indices of African aridity indicate a change to more arid conditions at this time[12]. In addition, the rate of loess deposition in China increased and the loess/palaeosol alternations began to correlate with the ice-volume record ($r = 0.7$ from 0.0–1.5 Myr ago and $r = 0.15$ from 1.5–2.5 Myr ago) at 1.5 Myr ago[13]. Although sustained high-amplitude glacial cycles did not begin until about 1.2 Myr ago[5], we suggest the transition to a climate regime conducive to sustained 100-kyr ice-sheet variability occurred 1.5 Myr ago.

One explanation for the high-amplitude climate response to low-amplitude orbital forcing is that the 100-kyr glacial cycles are a free oscillation internal to the climate system with the phase set by Milankovitch forcing[14,15]. If so, ice-sheet nonlinearities would contribute to a climate system that is inherently sensitive to forcing at eccentricity periods. However, this hypothesis does not adequately explain why 100-kyr climate fluctuations exist in a number of pre-Pleistocene climate records when large ice sheets were not available to provide the 100-kyr sensitivity, or when ice sheets were oscillating at other frequencies[16,17].

Some numerical models also require an approximately 10-kyr free oscillation or time constant that is internal to the model and dependent on free parameters[4,14,15]. For example, when a model[4] was run without an internal ~10-kyr oscillation the 100-kyr response to weak eccentricity forcing was correspondingly small. Subsequent adjustment of the free parameters in the model produced an internal, unforced ~10-kyr cycle. Model runs with the internal ~10-kyr oscillation and the weak eccentricity forcing produced a much larger 100-kyr response to weak eccentricity forcing. This result is consistent with resonance of a nonlinear oscillator to additive forcing[4]. Another model demonstrated a strong linkage between low-latitude semiprecession and 100-kyr cycles[18]. In the model output, the amplitude of the eccentricity-band spectral peaks is proportional to the amplitude of the semiprecession band spectral peaks.

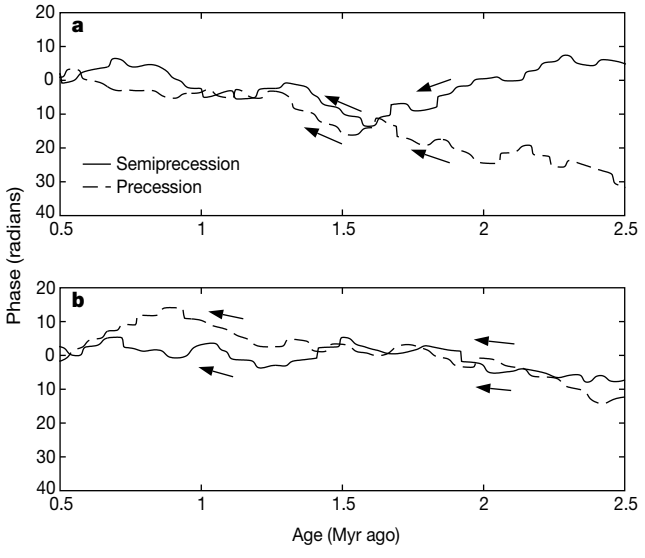

Figure 2 Instantaneous phase determined by complex demodulation. **a**, Phase of Site 607 $CaCO_3$ mass accumulation at precession and semiprecession frequencies. We note that before 1.5 Myr ago the phases move in opposite directions, indicating independence. After 1.5 Myr ago the phases move in the same direction, indicating they are coupled. **b**, Phase of Site 659 dust flux at precession and semiprecession frequencies. The phases are coupled throughout the entire 2.6-million-year record.

Our bispectral analyses (see Methods) suggest that semiprecession cycles, which are phase-coupled to precession and eccentricity, may provide the ~10-kyr oscillation needed by these climate models to produce 100-kyr ice-volume cycles. If this is the case, we would expect that the phase coupling between precession, semiprecession and eccentricity, which originates in the tropics, propagated to the high latitudes near the onset of 100-kyr glacial cycles.

A previous study used bispectral analysis to show that phase couplings similar to those in the insolation solutions were present in ice-volume records from 0 to 1.0 Myr ago but not from 1.0 to 2.6 Myr ago[8]. To further investigate these phase couplings we examined $CaCO_3$ mass accumulation rate (MAR) estimates from Deep Sea Drilling Project (DSDP) North Atlantic Site 607 (41° N, 32° W) (Fig. 1b) and dust accumulation estimates from Ocean Drilling Program (ODP) tropical Atlantic Site 659 (18° N, 21° W) on the same age model (Fig. 1c) (see Methods)[19]. The results of our bispectral analysis of these time series suggest that the phase-coupled characteristic of the tropical semiprecession cycles propagated to the North Atlantic between 1.2 and 1.9 Myr ago (see Methods).

If two frequencies are phase-coupled, as indicated by the bispectrum, then the instantaneous phases of the two frequencies (which can be determined by complex demodulation) should change in unison over time. Complex demodulation of the Site 607 $CaCO_3$ MAR at precession and semiprecession periods indicates that these two frequencies were phase-coupled in the North Atlantic between 0.5 and ~1.5 Myr ago but not before ~1.5 Myr ago (Fig. 2). This result is supported by a change in the character of the $CaCO_3$ MAR record near 1.5–1.6 Myr ago (Fig. 1b). In contrast, complex demodulation of the Site 659 dust flux record indicates that the precession and semiprecession periods were phase-coupled in the tropical Atlantic for at least the last 2.6 Myr, confirming the bispectral results. These results suggest that phase-coupled semiprecession cycles, which originate in the tropics, propagated to the high latitudes near 1.5 Myr ago, the same time that persistent 100-kyr ice-volume cycles began to build (Fig. 1a).

There are two ways to generate semiprecession cycles that are phase-coupled to precession and eccentricity. First, the alignment of perihelion with each equinox during one precession cycle produces a semiprecession cycle, analogous to the semiannual cycle produced by the passage of the sun over the equator twice each year. An energy balance model[18] demonstrated this process and its ability to produce power at 100- and 400-kyr periods. When semiprecession cycles occurred in the model output, 100-kyr cycles also occurred, with power proportional to that of the semiprecession cycle. In this case tropical heat export (either atmospheric or oceanic) can propagate the semiprecession signal from low to high latitudes[18]. Second, because the Northern and Southern hemispheres are 180° out of phase with respect to precession, the export of a Southern Hemisphere precession signal to the Northern Hemisphere will produce a semiprecession cycle in the Northern Hemisphere. Today, a Southern Hemisphere annual signal is exported to the Northern Hemisphere in the western tropical Atlantic where the south equatorial current is diverted into the Northern Hemisphere at Point Calcanhar, Brazil. Case two is similar to case one in that both require two precession cycles that are 180° out of phase. In case one, the cycles occur when perihelion is aligned with each equinox, whereas for case two they occur when perihelion is aligned with each solstice.

An annual analogue for both cases occurs in the tropical Atlantic. For case one, the passage of the sun over the equator twice per year produces a semiannual cycle, just as alignment of an equinox with perihelion twice during each precession cycle produces a semiprecession cycle. A semiannual cycle is documented in an empirical orthogonal function analysis of tropical Atlantic sea surface temperature (SST). In this analysis the second eigenvector exhibits

semiannual SST cycles with SST maxima occurring during both boreal spring and boreal autumn[20].

The export of a seasonal signal from the Southern to the Northern Hemisphere is an annual analogue for case two because the hemispheres are 180° out of phase with respect to both the seasonal and precessional cycles. Between 20° N and 20° S in the Atlantic Ocean, total monthly heat content peaks during austral summer and generally follows the Southern Hemisphere annual cycle[21]. In the northern tropical Atlantic (0° to 20° N), however, a second heat content peak occurs during boreal summer. In addition, the eastern equatorial Atlantic (6° N to 6° S) exhibits periods of heat export during both boreal summer and austral summer. Thus a semiannual cycle exists in the northern tropical Atlantic owing to the cross-equatorial influence of the Southern Hemisphere. Furthermore, tropical Atlantic SST and evaporative heat flux are important components in modelling the phase of the North Atlantic oscillation[22] which in turn influences the production of NADW on interannual to decadal timescales.

There is evidence that the semiannual analogue of heat export and SST in the eastern tropical Atlantic applies to semiprecession cycles. Estimates of SST and thermocline depth (an important factor in heat storage and export) in the tropical Atlantic over the last 20 kyr show two peaks approximately 10 kyr apart[23]. The double peak is particularly strong in the east, as in the semiannual analogue. In addition, zonal wind-driven divergence in the equatorial Atlantic over the past 40 kyr exhibits a dominant periodicity near that of semiprecession[24].

The African and Asian monsoons provide another means of producing semiprecession cycles. Previous studies showed that the strength of the Asian monsoon is in phase with a Southern Hemisphere latent heat source at the precession period[11] while the African monsoon is in phase with maximum Northern Hemisphere summer insolation[25]. Neither of these studies examined the phase of semiprecession cycles, but they suggest that monsoon strength depends on sensible heating of the continent in the Northern Hemisphere and latent heat transported from the Southern Hemisphere. Northern Hemisphere sensible heating is greatest when boreal summer is aligned with perihelion and Southern Hemisphere latent heat export is greatest one-half precession cycle later, when boreal summer is aligned with aphelion and atmospheric circulation during austral winter is strongest[11]. By shifting the balance of these monsoon drivers, it may be possible to vary the intensity of a semiprecession cycle in the Northern Hemisphere.

Recent modelling studies of orbitally-forced El Niño variability provide additional support for a tropical driver of ice-sheet variability[26]. The model output shows that El Niño frequency and intensity varies at precession and semiprecession periods. Extending the modern El Niño effects on Hadley circulation, poleward heat transport, and high-latitude North American seasonality to longer timescales suggests that tropical teleconnections may be important in the growth and decay of large Northern Hemisphere ice sheets[26].

Our results indicate that a major climate threshold was crossed near 1.5 Myr ago; a time marked by large changes in low-latitude terrestrial conditions[11,13,25] and in thermohaline circulation[9,10]. Our results also suggest that enhancement of either low- to high-latitude climate connections (case 1) or cross-equatorial heat flow (case 2) initiated the growth of 100-kyr ice sheets at that time. In either case, our results suggest that the tropics played a major role in the initiation and maintenance of the 100-kyr ice-sheet oscillations of the last 1.5 million years. □

Methods

Data

We placed the Site 607 $CaCO_3$ and Site 659 dust accumulation records on the oxygen isotope[2,27] age model from Site 659 (ref. 19). Although weight per cent $CaCO_3$ at Site 607 is strongly influenced by ice-rafted detritus (IRD) during the past 2.5 Myr (ref. 28), $CaCO_3$ MAR depends on dissolution at depth and $CaCO_3$ production in the surface waters and is independent of dilution by IRD. The Site 659 dust flux record is a particularly relevant tropical record because low-latitude land masses should exhibit strong semiprecession variability[18].

Signal processing

Bispectral analysis is a signal processing technique that detects phase coupling between different frequencies in a single time series. Bispectral analysis of Site 607 $CaCO_3$ MAR shows significant North Atlantic phase couplings between precession, eccentricity, and semiprecession from 0.2 to 1.2 Myr ago but not from 1.9 to 2.9 Myr ago. However, bispectral results for ODP Site 659 (18° N, 21° W) dust flux[19] indicate that significant tropical phase couplings existed during both time intervals.

Like spectral analysis, the results of bispectral analysis are averaged over the length of the time series and it is difficult to constrain the timing of transitions. To determine the timing of the transition to a phase-coupled system in the North Atlantic, we used complex demodulation to extract the instantaneous phase of the phase-coupled frequencies determined by bispectral analysis. Demodulation was performed using the ARAND package on phase-locked precession and semiprecession periods as indicated by the bispectral results. For Site 607 these were 19 and 9.5 kyr which show strong phase couplings with each other and with eccentricity over the past 1.6 million years. For Site 659 the demodulation isolated periods of 21 and 10.5 kyr. These two periods are strongly phase-coupled with each other and with eccentricity throughout the past 2.6 million years. A filter with 100 weights, a half-amplitude frequency of 0.01 cycles per kyr and a stop frequency of 0.016 cycles per kyr was used on all demodulations. The filter satisfies two requirements[29]: it passes all frequencies out to one-half the precession (or semiprecession) bandwidth (~0.0078); and it safely stops all harmonics, which begin at a frequency of 0.028 after demodulation (for example, the first precession harmonic 1/12 kyr to 1/18 kyr).

Received 2 February; accepted 5 September 2000.

1. Raymo, M. E., Ruddiman, W. F. & Clement, B. M. in *Initial Reports Deep Sea Drilling Project: Leg 96* (eds Ruddiman, W. F. *et al.*) 895–901 (US Government Printing Office, Washington DC, 1986).
2. Ruddiman, W. F., Raymo, M. E., Martinson, D. G., Clement, B. M. & Backman, J. Pleistocene evolution: Northern Hemisphere ice sheets and North Atlantic Ocean. *Paleoceanography* **4,** 353–412 (1989).
3. Hays, J. D., Imbrie, J. & Shackleton, N. J. Variations in the earth's orbit: pacemaker of the ice ages. *Science* **194,** 1121–1131 (1976).
4. LeTreut, H. & Ghil, M. Orbital forcing, climatic interactions, and glaciation cycles. *J. Geophys. Res.* **88,** 5167–5190 (1983).
5. Chen, J., Farrell, J. W., Murray, D. W. & Prell, W. L. Timescale and paleoceanographic implications of a 3.6 m.y. oxygen isotope record from the northeast Indian Ocean (Ocean Drilling Program site 758). *Paleoceanography* **10,** 21–47 (1995).
6. Park, J. & Maasch, K. A. Plio-Pleistocene time evolution of the 100-kyr cycle in marine paleoclimate records. *J. Geophys. Res.* **98,** 447–461 (1993).
7. Rial, J. A. Pacemaking the ice ages by frequency modulation of Earth's orbital eccentricity. *Science* **285,** 564–569 (1999).
8. Hagelberg, T., Pisias, N. & Elgar, S. Linear and nonlinear couplings between orbital forcing and the marine $\delta^{18}O$ record during the Late Neogene. *Paleoceanography* **6,** 729–746 (1991).
9. Raymo, M. E., Ruddiman, W. F., Shackleton, N. J. & Oppo, D. W. Evolution of Atlantic-Pacific $\delta^{13}C$ gradients over the last 2.5 m.y. *Earth Planet. Sci. Lett.* **97,** 353–368 (1990).
10. Bickert, T., Cordes, R. & Wefer, G. in *Proceedings of the Ocean Drilling Program, Scientific Results, Leg 154* (eds Shackleton, N. J., Curry, W. B., Richter, C. & Bralower, T. J.) 229–237 (Ocean Drilling Program, College Station, Texas, 1997).
11. Clemens, S. C., Murray, D. W. & Prell, W. L. Nonstationary phase of the Plio-Pleistocene Asian monsoon. *Science* **274,** 943–948 (1996).
12. deMenocal, P. & Bloemendal, J. in *Paleoclimate and Evolution with Emphasis on Human Origins* (eds Vrba, E. S., Denton, G. H., Partridge, T. C. & Burckle, L. H.) 262–288 (Yale Univ. Press, New Haven, Connecticut, 1995).
13. Bloemendal, J., Liu, X. M. & Rolph, T. C. Correlation of the magnetic susceptibility of Chinese loess and the marine oxygen isotope record: Chronological and palaeoclimatic implications. *Earth Planet. Sci. Lett.* **131,** 371–380 (1995).
14. Maasch, K. A. & Saltzman, B. A low-order dynamical model of global climatic variability over the full Pleistocene. *J. Geophys. Res.* **95,** 1955–1963 (1990).
15. Saltzman, B. & Verbitsky, M. Late Pleistocene climate trajectory in the phase space of global ice, ocean state, and CO_2: Observations and theory. *Paleoceanography* **9,** 767–779 (1994).
16. Herbert, T. D. & Fischer, A. G. Milankovitch climate origin of mid-Cretaceous black shale rhythms in central Italy. *Nature* **321,** 739–743 (1986).
17. D'Hondt, S., King, J. & Gibson, C. Oscillatory marine response to the Cretaceous-Tertiary impact. *Geology* **24,** 611–614 (1996).
18. Short, D. A., Mengel, J. G., Crowley, T. J., Hyde, W. T. & North, G. R. Filtering of Milankovitch cycles by Earth's geography. *Quat. Res.* **35,** 157–173 (1991).
19. Tiedemann, R., Sarnthein, M. & Shackleton, N. J. Astronomic timescale for the Pliocene Atlantic $\delta^{18}O$ and dust flux records from Ocean Drilling Program Site 659. *Paleoceanography* **9,** 619–638 (1994).
20. Servain, J. & Legler, D. M. Emperical orthogonal function analysis of tropical Atlantic sea surface temperature and wind stress: 1964–1979. *J. Geophys. Res.* **91,** 14181–14191 (1986).
21. Merle, J. Seasonal variation of heat-storage in the tropical Atlantic Ocean. *Oceanol. Acta* **3,** 455–463 (1980).
22. Rodwell, M. J., Rowell, D. P. & Folland, C. K. Oceanic forcing of the wintertime North Atlantic Oscillation and European climate. *Nature* **398,** 320–323 (1999).
23. Molfino, B. & McIntyre, A. Nutricline variation in the equatorial Atlantic coincident with the Younger Dryas. *Paleoceanography* **5,** 977–1008 (1990).
24. McIntyre, A. & Molfino, B. Forcing of Atlantic equatorial and subpolar millennial cycles by precession. *Science* **274,** 1867–1870 (1996).
25. deMenocal, P. B. Plio-Pleistocene African climate. *Science* **270,** 53–59 (1995).

26. Clement, A., Seager, R. & Cane, M. Orbital controls on the El Nino/Southern Oscillation and the tropical climate. *Paleoceanography* **14,** 441–456 (1999).
27. Raymo, M. E., Ruddiman, W. F., Backman, J., Clement, B. M. & Martinson, D. G. Late Pliocene variation in Northern Hemisphere ice sheets and North Atlantic Deep Water circulation. *Paleoceanography* **4,** 413–446 (1989).
28. Ruddiman, W. F. & Raymo, M. in *Initial Reports of the Deep Sea Drilling Project: Leg 96* (eds Ruddiman, W. F., Kidd, R. B. & Thomas, E.) 855–878 (US Government Printing Office, Washington, 1986).
29. Bloomfield, P. *Fourier Analysis of Time Series: An Introduction* 1–258 (Wiley, New York, 1976).
30. Ruddiman, W. F., Kidd, R. B., Thomas, E. *et al. Initial Reports of the Deep Sea Drilling Program: Leg 96* 1251 (US Government Printing Office, Washington DC, 1987).

Acknowledgements

We thank R. Tiedemann for providing the data from Site 659 and M. Raymo for data from Site 607. K. Maasch and M. E. Mann provided helpful comments. This work was supported by the National Science Foundation.

Correspondence and requests for materials should be addressed to S.R. (e-mail:srutherford@gso.uri.edu).

Accelerated hydration of the Earth's deep crust induced by stress perturbations

Bjørn Jamtveit, Håkon Austrheim & Anders Malthe-Sørenssen

The Fluid Rock Interaction Group, Departments of Geology & Physics, University of Oslo, PO Box 1047 Blindern, N-0316 Oslo, Norway

The metamorphic cycle associated with the formation of mountain belts produces a lower crust containing little or no free fluid[1,2]. The introduction of external fluids to dry and impermeable volumes of the Earth's crust is thus a prerequisite for the retrogressive metamorphism later observed in such regimes. Such metamorphism can cause significant changes in the crust's physical properties, including its density, rheology and elastic properties[3,4]. On a large scale, the introduction of fluids requires the presence of high-permeability channels, such as faults or fractures, which are the result of external tectonic stresses. But extensive interaction between externally derived fluids and the fractured rock requires efficient mass transport away from the initial fractures into the rock itself, and this transport often occurs over distances much longer than expected from grain-boundary diffusion. Here we present both field observations and a simple network model that demonstrate how the transport of fluids into initially dry rock can be accelerated by perturbations in the local stress field caused by reactions with fluids. We also show that the morphology of reaction fronts separating 'dry' from 'wet' rocks depends on the anisotropy of the external stress field.

'Dry' volumes of the Earth's crust contain no separate fluid phase although both the mineral surfaces and crystal lattices are likely to contain more or less strongly adsorbed volatile components. Reactions between volatiles and such dry rocks may occur at any depth in the Earth's crust at which externally derived fluids get access to the rocks at a temperature where hydrous phases or carbonates are stable. An excellent field example of such a process can be found in the Bergen Arcs of southwestern Norway. The Bergen Arcs are a series of arcuate Caledonian nappes thrust upon the Proterozoic basement rocks of the western gneiss region of western Norway[5] (Fig. 1).

One of these, the Lindaas nappe, consists mainly of dry Proterozoic granulite facies rocks, including anorthosites, that were partly hydrated during the Caledonian orogeny some 420 Myr ago[6]. The hydration occurred both under eclogite and amphibolite facies metamorphic conditions. Figure 2a shows how a reaction front defining the transition from dry anorthosite to hydrated ('wet') eclogite surrounds a fracture that initially formed within the anorthosite. This fracture is filled with a vein assemblage consisting of euhedral omphacite in a matrix of quartz, clinozoisite, phengite, plagioclase and kyanite that precipitated from the externally introduced fluid at a temperature around 700 °C and a pressure around 1.5 GPa (ref. 7).

Phase petrological analyses indicate that the fluid was water-rich (>50 mol.% H_2O)[7]. Apart from a kink fold centred on the fracture or vein (Fig. 2a), there is no extensive internal deformation within the eclogitized part of the anorthosite, and the front separating the anorthosite from the eclogite is flat and morphologically stable on the macroscale. The transition from anorthosite to eclogite involves

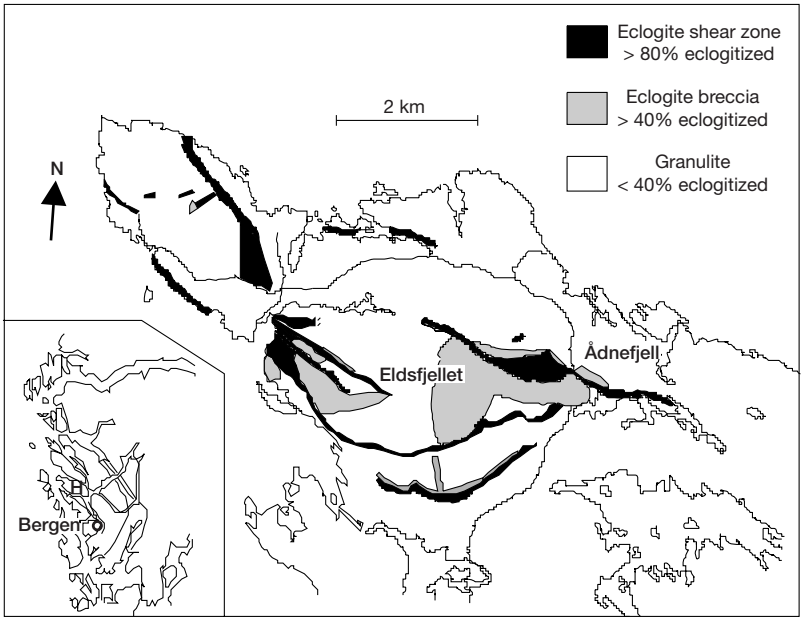

Figure 1 Geological map of Holsnøy northwest of Bergen in western Norway. Holsnøy is labelled H in the inset. Non-shaded regions are composed of 'dry' granulite facies rocks, notably anorthosites. Shadings denote areas with different extents of eclogitization (hydration under eclogite facies conditions).